

Picosecond Timing Resolution Measurements of Low Gain Avalanche Detectors with a 120 GeV Proton Beam for the TOPSiDE Detector Concept

M. Jadhav^{a,*}, W. Armstrong^a, I. Cloet^a, S. Joosten^a, S. M. Mazza^b, J. Metcalfe^a, Z.-E. Meziani^a, H.F.-W. Sadrozinski^b, B. Schumm^b, A. Seiden^b

^a*Argonne National Laboratory, IL 60439, USA*

^b*Santa Cruz Institute for Particle Physics UC Santa Cruz, CA 95064, USA*

Abstract

This paper presents results that take a critical step toward proving 10 ps timing resolution's feasibility for particle identification in the TOPSiDE detector concept for the Electron-Ion Collider. Measurements of LGADs with a thickness of 35 μm and 50 μm are evaluated with a 120 GeV proton beam. The performance of the gain and timing response is assessed, including the dependence on the reverse bias voltage and operating temperature. The best timing resolution of UFSDs in a test beam to date is achieved using three combined planes of 35 μm thick LGADs at -30 °C with a precision of 14.31 \pm 1.52 ps.

Keywords: Silicon, Charge Multiplication, Thin sensors, Ultra-Fast Silicon Detectors, Low-Gain Avalanche Detectors

*Corresponding author

Email address: mjadhav@anl.gov (M. Jadhav)

1. Introduction

Ultra-Fast Silicon Detectors (UFSD) [1] are a novel type of silicon detector that simultaneously provides both spatial and timing resolution. One kind of UFSD, the Low-Gain Avalanche Detector (LGAD) [2], relies on an internal charge multiplication mechanism, or an avalanche effect, that is introduced in a controlled manner by the implantation of an appropriate acceptor or donor dopant layer. The internal charge multiplication process provides a moderate internal gain that increases the detector signal output, which further increases the signal-to-noise (S/N) ratio [3].

UFSDs are targeted at a range of new opportunities from space science, mass spectroscopy, medical science to nuclear and particle physics [4]. The precision timing measurement combined with the high granularity spatial measurement enables a 4-Dimensional detector concept for particle detectors. A precise timing response translates into excellent time-of-flight (ToF) measurements, thus providing good particle identification (PID). The Timing Optimized PID Silicon Detector (TOPSiDE) concept [5–7] for the Electron-Ion Collider (EIC) is one such application. It implements a 4D concept with precision timing of the order of 10 ps. This enables pion/kaon separation up to 7 GeV/ c using ToF method at up-to efficiency of 90% [8]. It provides the precision measurements required for the EIC’s broad physics program; some major topics include deep inelastic structure functions of protons and nuclei, spin structure functions, generalized parton distributions (GPDs), and transverse momentum dependent distributions (TMDs) [9]. The results here demonstrate 15 ps timing resolution with three layers of 35 μm thick sensors. It is expected that with thinner sensors, the 10 ps goal is readily achievable.

2. Low Gain Avalanche Detectors

LGADs are distinguished from traditional silicon sensors by the gain layer beneath the electrode contacts, as shown in figure 1. The charge carrier collection time inside the silicon is limited by saturation of electron drift velocity at about 10^7 cm/s and takes ~ 1 ns to collect the charge for a ~ 100 μm thick sensor [1, 10]. The thicker sensors are required to keep the S/N to a level acceptable to the electronics. An LGAD relies on a gain layer to increase the signal by a factor of 10 to 100, allowing thinner sensors and a shorter drift distance and collection time [1, 10].

The first LGAD was fabricated by Centro Nacional de Microelectrónica (CNM-IMB), Barcelona, Spain with a thickness of 300 μm and maximum

gain of 10 at 300 V for $-10\text{ }^{\circ}\text{C}$ [2]. The timing resolution of the order of 100 ps is reported for these sensors [11, 12]. Since then, several LGADs with much thinner thickness and improved gain have been studied [11, 13]. The best timing precision recorded so far with a single UFSD under test is 18 ps for LGAD with a thickness of $50\text{ }\mu\text{m}$ and the gain of ~ 70 at $-20\text{ }^{\circ}\text{C}$ [14]. The paper [15] also reported the timing resolution of $17 \pm 1\text{ ps}$ for trigger UFSD. The best timing precision in a test beam scenario was found to be 27 ps with a single LGAD sensor with thickness $45\text{ }\mu\text{m}$ (gain 70) [3] and $50\text{ }\mu\text{m}$ (gain 27) [16] at 180 GeV pion beam at CERN. The best timing reported with three $45\text{ }\mu\text{m}$ LGADs together in test beam set-up is 16 ps [3].

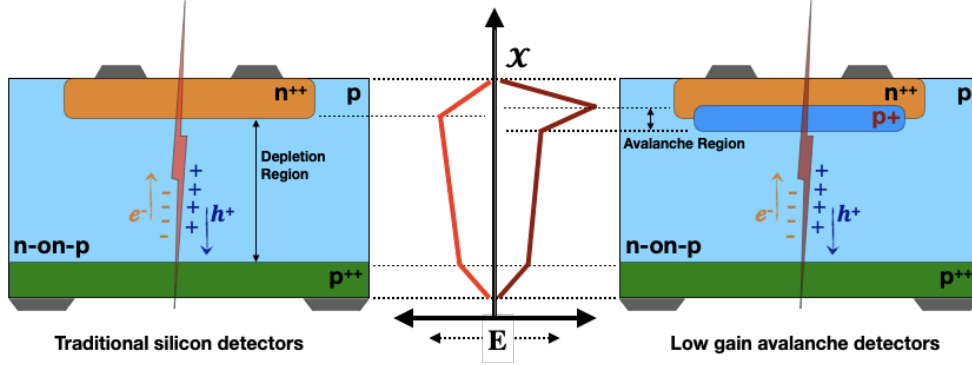


Figure 1: Comparison between (left) traditional silicon detector and (right) low-gain avalanche detector.

3. Experimental setup

Measurements of several types of LGADs are performed with a 120 GeV proton beam at the Fermilab Test Beam Facility (FTBF). The trigger sensor's timing resolution is measured using ^{90}Sr β -telescope setup in the laboratory. The UFSD devices are characterized for charge collection efficiency, gain, and timing resolution for different bias voltages and temperatures. The following section describes the samples and test setup.

3.1. LGAD Devices and Electrical properties

The LGADs with different thicknesses, doping concentrations, and sensor types (pad, pixels, strips, AC-LGADs) have been measured for timing resolution and radiation hardness. The LGADs tested and presented in this

paper are manufactured by Hamamatsu Photonics K.K. (HPK) and tagged as HPK-1.2 and HPK-3.1. The sensors are *n-on-p* type with a thickness of 35 μm and 50 μm , respectively, whereas the physical thickness, including substrate wafer, varies between 300 to 350 μm . HPK1.2 and HPK3.1 both have an active pads area of $1.3 \times 1.3 \text{ mm}^2$. Both the LGADs are doped with Boron to create an internal multiplication layer. HPK-1.2 has shallow implantation and higher resistivity with a breakdown voltage of around 270 V. The HPK-3.1 has deeper implantation with a breakdown voltage slightly above 245 V. The capacitance of the LGADs vary with the total active bulk and doping profile. It is measured to be 5.35 pF and 3.9 pF for LGADs HPK-1.2 and HPK-3.1, respectively. The detailed description of the LGADs can be found in references [17–20].

Table 1: The description of LGAD devices under test.

Sensors HPK	Type	Thickness (μm)	Pad Area (mm^2)	C (pF)	Rise Time (10-90%)	Breakdown Voltage
3.1	<i>n-on-p</i>	50	1.3×1.3	3.9	470 ps	245 V
1.2	<i>n-on-p</i>	35	1.3×1.3	5.35	375 ps	270 V

Additionally, an HPK8664, a *p-on-n* type LGAD sensor, is evaluated. The HPK8664 has a round pad with a circular area of about 1 mm^2 without any guard ring protection. With the breakdown voltage of 430 V, this sensor is used as a trigger during data taking.

3.2. Sample Setup

The LGAD sensors were mounted on a $\sim 10 \times 10 \text{ cm}^2$ read-out board, shown in figure 2(b). The single-channel read-out board contains wide bandwidth ($\sim 2 \text{ GHz}$) and low noise inverting amplifier with a gain of 10 and has been used in previous studies[1, 3]. The inverting amplifier is followed by a second stage 2 GHz external amplifier with gain 10. The combined trans-impedance of the read-out is about 4700Ω .

The sensors are glued to the 5 mm square pad on the read-out board with the guard ring is grounded. Two or more read-out boards are aligned back-to-back, as shown in the figure 2(a) using alignment rods passing through the holes at each corner of the alignment frame and read-out boards. The

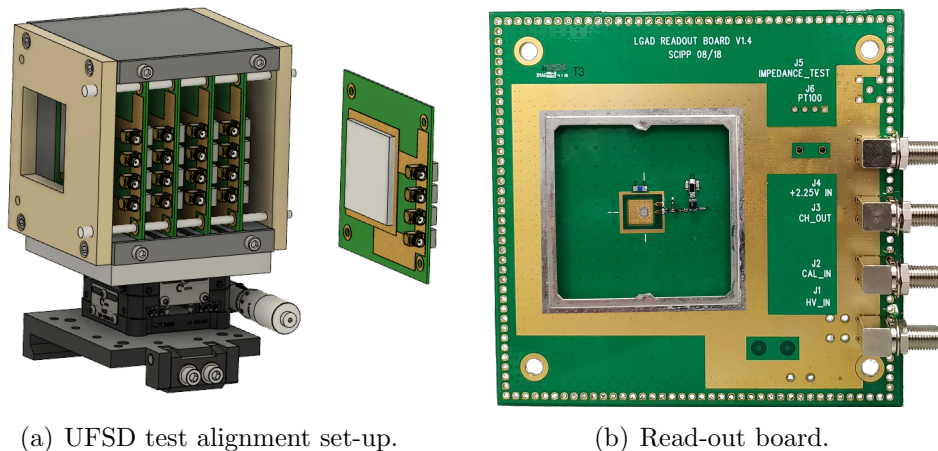


Figure 2: The alignment frame (left) and read-out front-end board with discrete components to collect the signal (right).

alignment box is designed to use up to four sample boards. The alignment box is used in both setups, the ^{90}Sr β -Telescope and test beam measurements as shown in the figure 3(a) and 3(b) respectively. In each case, the incident particle radiations pass perpendicularly through the sample boards and the sensors' active region. A window in the sides of the box prevents the absorption/energy loss of the incoming particle.

In each case, one sensor is designated the trigger sensor (TRG), and the other sensors are considered the devices under test (DUT). The samples are biased using CAEN DT1471ET high voltage supply. The amplified signal from the read-out is recorded using a 2.2 GHz Keysight DSOS204A digital oscilloscope. The sampling rate is 20 GSa/s with time discretization of 50 with two active channels. In contrast, the sampling rate reduces to 10 GSa/s with time discretization of 100 while using all four oscilloscope channels. The events are registered for all DUTs when the trigger sensor fires to provide a signal above the threshold value. The oscilloscope captures the events as a signal pulse waveform. The raw data is acquired and stored in a computer using a Python-based PyVisa interface, referred to as the DAQ framework.

3.3. ^{90}Sr β -Telescope Setup

The ^{90}Sr β -source measurements are performed by mounting the source in the alignment box. The β -source can only penetrate two sensors before being absorbed. Thus, only two oscilloscope channels are used, allowing for

a 20 GSa/s sampling rate. Cold measurements are done by placing the setup in an environmental chamber.

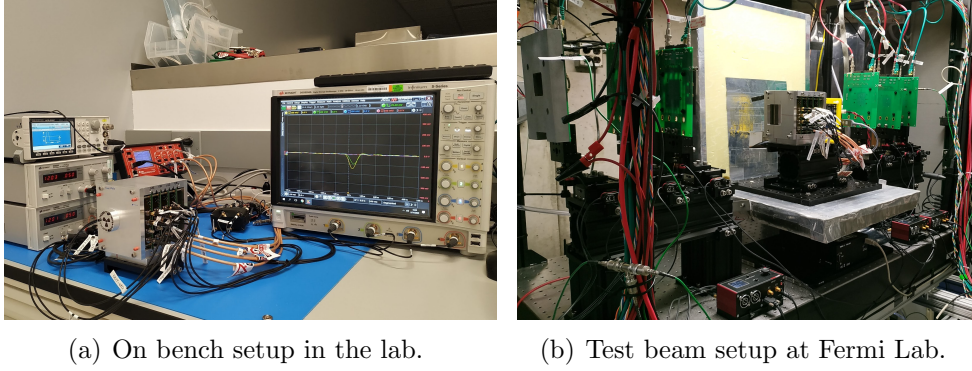


Figure 3: Test setup for timing measurement of LGADs using time-of-flight (TOF) technique for minimum ionizing particles (MIP) using Sr^{90} source in the lab (left) and at the Fermi lab test beam facility (right).

3.4. Fermilab Test Beam Setup

The test beam measurements are performed at the Fermilab Test Beam Facility (FTBF) using a 120 GeV proton beam [21]. For the test beam campaign, four LGAD sensors are used simultaneously utilizing all four channels of the oscilloscope. However, this limits the sampling rate to 10 GSa/s with a time discretization of 100 ps. The time resolution measurements are compared to those with a sampling rate of 20 GSa/s, and the results are consistent. The trigger sensor is the fourth LGAD sensor in the alignment box placed downstream in the beamline. The data is acquired at room temperature for both the UFSDs. The low-temperature measurements also performed for the HPK-1.2 at $-30\text{ }^{\circ}\text{C}$ of air temperature inside the enclosure. The system is housed in a cold box that maintains a low temperature using a cold plate cooled by a Julabo FP89-ME recirculating chiller. The humidity inside the box is kept below the dew point by using Nitrogen purging.

The test beam data is collected in spills of 4 seconds duration per minute. The beam's intensity is kept between 100K to 200K protons every spill with the circular beam spot with 2-4 mm σ -value. The beam is adjusted to get an instantaneous trigger rate between 1 and 10 Hz. All the DUTs in the setup are operated at the same bias voltage. The data is acquired at biases

ranging from 200 V to 255 V for UFSDs; HPK-1.2, and HPK-3.1 at different temperature conditions. The maximum bias voltage is defined by the breakdown conditions for particular UFSD and temperature. The trigger is supplied with a fixed bias voltage of 425 V throughout the test beam run. The leakage current through all the sensors was stable at around 15-25 nA during the test run.

Figure 4 shows an example of one of the events at a test beam run where all four UFSDs are fired. In the event, all four HPK-1.2 UFSDs are operated at a bias voltage of 250 V with a leading-edge time around 350 ps.

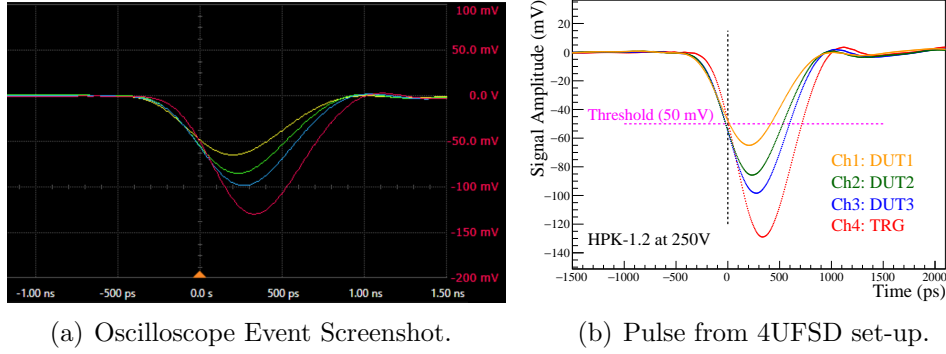


Figure 4: The event with signal pulse from TRG and DUT. As detectors are aligned back-to-back, such events are considered to be from minimum ionizing particles (MIP).

4. Data Analysis Method

The data analysis follows a similar procedure as [3, 15]. It uses only those variables which would be available with a hypothetical read-out chip, like time-of-arrival (ToA), signal amplitude, and time-over-threshold (ToT). The time at which the signal pulse crosses a certain fraction of the maximum signal amplitude is considered time-of-arrival. The corresponding amplitude is referred to as CFD value. For example, `cfid[20]` indicates the time with CFD value equals to 20% of maximum pulse amplitude. The information plays a critical role in calculating different parameters, like the time difference between DUT and trigger, rise time, jitter, etc. The method is called a constant fraction discriminator (CFD) method. It is proven to be highly effective in correcting the time-walk effect by overcoming the limitation imposed by the

oscilloscope digitization. Figure 5(a) shows the calculation of CFD value and the corresponding time using a linear interpolation method. The distribution of time at different CFD values (fractions) and its comparison with signal waveform data is shown in figure 5(b).

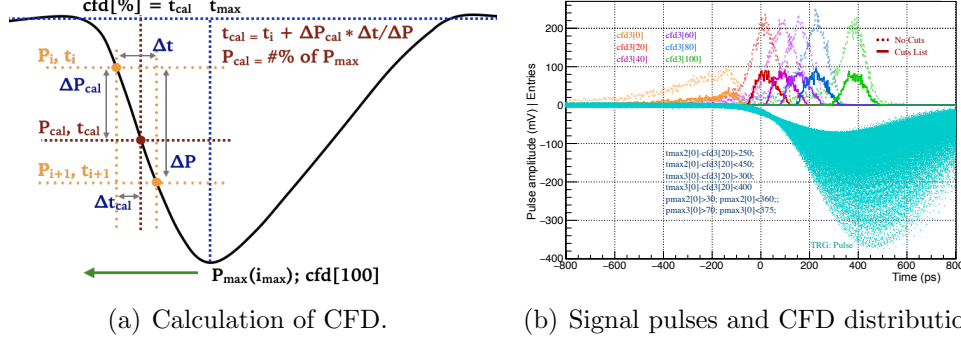


Figure 5: The calculation of CFD value by linear interpolation method provides the timing information at a certain fraction of maximum signal amplitude (left). The time distribution at different CFD values compared to signal waveform data for the HPK-8664 trigger detector at bias voltage 425V taken in the laboratory with ^{90}Sr β -source (right). The dotted lines show distribution before event selection, and the solid line denotes distribution for selected events.

The selection criteria applied to events with a valid trigger pulse are mainly based on signal amplitude and time of arrival. The maximum signal amplitude, P_{max} of all UFSDs, should be at least five times larger than the noise level, and the oscilloscope or the read-out chain should not saturate it. The second selection is on the time difference between the DUT and the trigger. The time difference criterion reduces the contribution from the non-gain events or noise. As shown in the upper panel of figure 5(b), the selection rules allow removing the low-gain tail effect on the distribution's left side. The figure 6 shows the amplitude selection along the horizontal axis and time selection along the vertical axis.

The selected data is analyzed to study the signal amplitude distribution, collected charge, the gain, the jitter, the rise time, and the timing resolution. The following sub-sections provide analysis details of these variables.

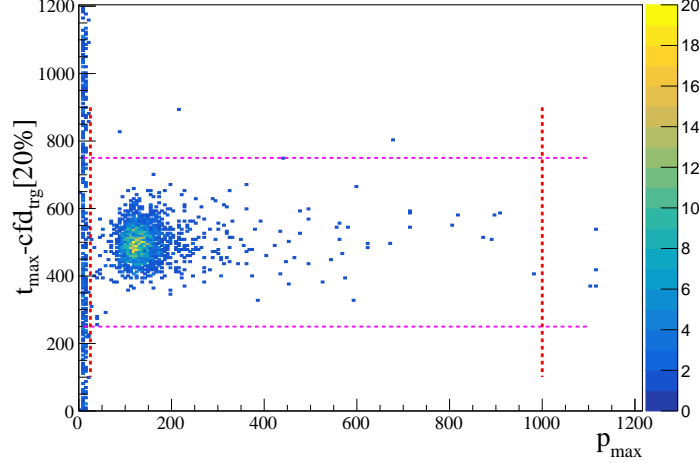


Figure 6: Event selection based on the distribution of time difference versus signal amplitude for DUT HPK-1.2 operated at bias voltage 250V with 120 GeV proton beam at Fermilab test beam facility.

4.1. Time Resolution

The time resolution, σ_t of the detector system can be expressed as a sum of different contributions [1, 22],

$$\sigma_t^2 = \sigma_{Jitter}^2 + \sigma_{LandauNoise}^2 + \sigma_{TimeWalk}^2 + \sigma_{Distortion}^2 + \sigma_{TDC}^2 \quad (1)$$

The CFD method is useful in compensating the effect of the time-walk. The signal distortion is negligible in silicon for the saturated drift velocity and uniform weighting field. It is achievable using "parallel plate" geometry with a large active area compared to sensor thickness [1]. The contribution from the time-to-digital (TDC) is equal to the timing uncertainty, $\Delta T/\sqrt{2}$. Where ΔT is the least significant bit of TDC. The TDC effect is minimal in most of the cases and ignored in this paper. The predominant contribution to the timing resolution is from Jitter and Landau Noise.

The Gaussian function is used to fit the time difference (Δt) distribution between the DUT and the trigger. The fitting parameter, $\sigma_{(DUT-TRG)}$ provides the timing resolution of the device under test using a quadrature.

$$\sigma_{DUT}^2 + \sigma_{TRG}^2 = \sigma_{(DUT-TRG)}^2. \quad (2)$$

Where σ_{DUT} and σ_{TRG} are the timing resolution of the DUT and the trigger, respectively. For a unique setup where DUT and TRG use the same

types of LGADs, the equation will be simplified as,

$$\sigma_{DUT} = \sigma_{(TRG-DUT)}/\sqrt{2}. \quad (3)$$

4.2. Charge Collected and Gain

The energy deposited by the minimum ionizing particles in the active bulk of the LGAD sensor follows the Landau distribution before getting amplified by the internal gain process.

The gain is given by the ratio of the initial number of charge carriers and the total charge after multiplication. The collected charge is calculated by dividing the pulse area by the input trans-impedance of the detector system. The pulse area is the integration of pulse waveform from 1 ns before the start of the pulse (i.e., zero-crossing) and 3ns after the pulse reaches its maximum amplitude (i.e., t_{max}). The Weight-Field2 simulation calculates the initial charge collection using an identical PIN sensor without a gain layer.

4.3. Jitter and Landau Fluctuation

Jitter is directly proportional to the noise and minimized by having a higher slew-rate and low intrinsic noise.

$$\sigma_{jitter} = \frac{Noise}{dV/dt}. \quad (4)$$

Wherein, the noise is determined as the RMS fluctuation of the oscilloscope's baseline trace and calculated using $1/4^{th}$ of total points in the waveform from the beginning of the pulse.

Another contribution to timing performance is Landau noise, which is introduced by a particle's non-uniform charge deposition along its passage. The Landau noise is insensitive to the gain value and found to be dependent on CFD settings. The Landau noise decreases with the thickness of the sensor [1, 23]. It has been observed that jitter and Landau noise contribute almost equally in time resolution for sensors with a thickness below 150 μm [1].

5. Laboratory Results

The goal is to find the timing resolution of HPK-8664, a trigger detector for the test beam campaign. The timing resolution of HPK-1.2 is measured using two identical LGADs. Figure 7(a) shows the timing difference at 50%

CFD fractions, and the timing resolution is calculated using equation 3. The HPK-1.2 provides a timing resolution of (29.03 ± 0.41) ps at bias voltage 250 V. Two LGADs, HPK-1.2, and HPK-8664 are used for laboratory testing. The timing resolution of HPK-8664 is then measured using HPK-1.2 as a trigger. The HPK-8664 is operated at a bias voltage of 425 V and HPK-1.2 at 250 V. For the set-up with two different types of UFSDs, the time difference is taken at two different but optimized values of CFD fractions, i.e., 20% CFD for HPK-8664 and 50% CFD for HPK-1.2 sensor. The timing resolutions of HPK8664 is calculated using equation 2. It is (27.39 ± 0.61) ps at bias voltage 425 V and room temperature. Whereas, at temperature -30°C , it is (24.22 ± 0.75) ps when operated at bias voltage 390 V.

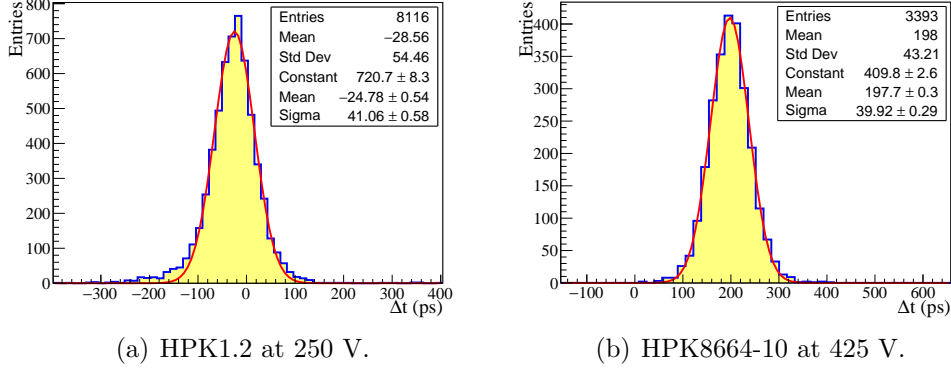


Figure 7: The distribution of time difference between the DUT and the trigger. (left) The DUT and the trigger both are HPK-1.2 operated at 250 V. (right) The time difference between HPK-8664 at 425 V and HPK-1.2 at 250 V.

6. Test Beam Results

6.1. Charge Collection and Gain

The charge collection performance of UFSDs as a function of the bias voltage is shown in figure 8(a). The rising trend indicates the increased rate of charge multiplication along with bias voltage. It also demonstrates that the charge multiplication rate increases with reduced temperature but also restricted by reduced breakdown voltage at low temperature. Figure 8(b) shows the gain as a function of bias voltage for HPK-1.2 and HPK-3.1. The results show the exponential dependence of internal gain on the electric field and subsequently

on the reverse bias voltage as expected in [1, 24]. At room temperature, the maximum gain of 76 (figure 8(b)) is achieved from HPK-1.2 biased at 255 V.

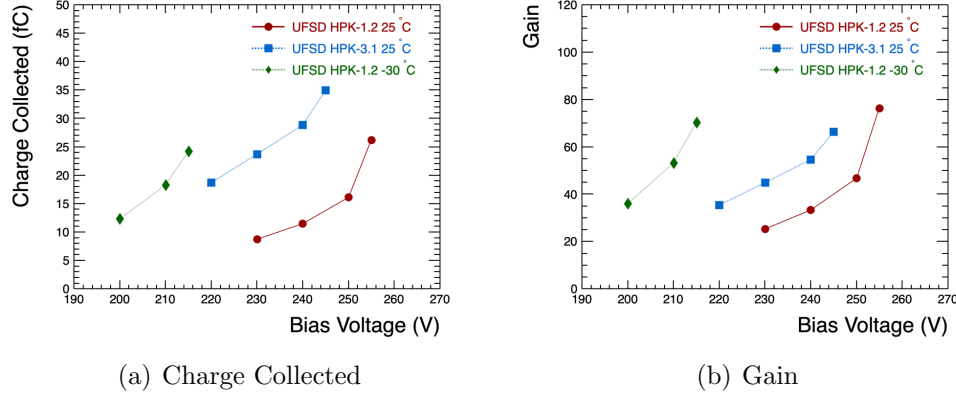


Figure 8: The charge collected (left) and the gain (right) as a function of bias voltage.

6.2. Signal Amplitude

In general, the energy deposited in the thin silicon sensor follows Landau distribution. The average signal shape at a different internal gain is shown in the figure 9(a). However, the distribution of signal amplitude shown in figure 9(b) exhibits the convolution of Landau with a Gaussian distribution. The studies performed with laser pulse imply that the Gaussian contribution is from the read-out board's impulse response [3]. The Landau distribution provides the most probable value (MPV) and Full Width Half Maximum (FWHM). Whereas, Gaussian width, σ_{Gauss} demonstrate the noise and fluctuations. The increase in the Gaussian width with bias voltage implies an increase in the contribution by noise from the amplifier and the sensor's shot noise. Figure 10 show the increasing trend of signal amplitude as a function of bias voltage for HPK-1.2 and HPK-3.1.

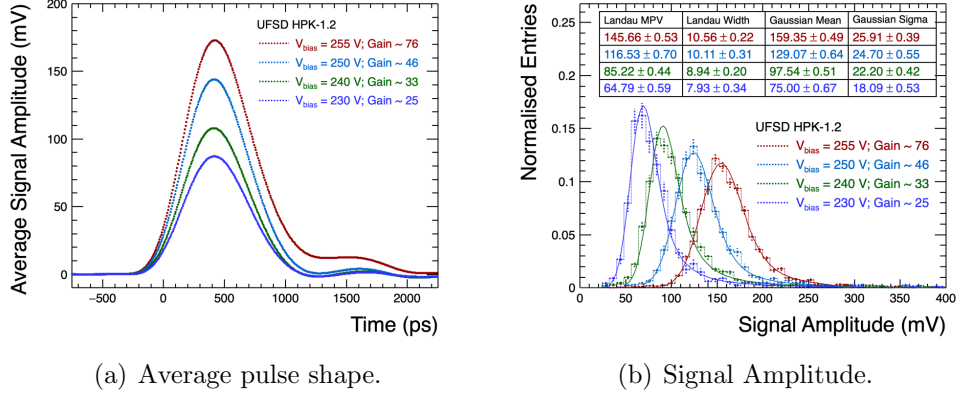


Figure 9: The average signal shape (left) and distribution of signal amplitude normalized by its integral (right).

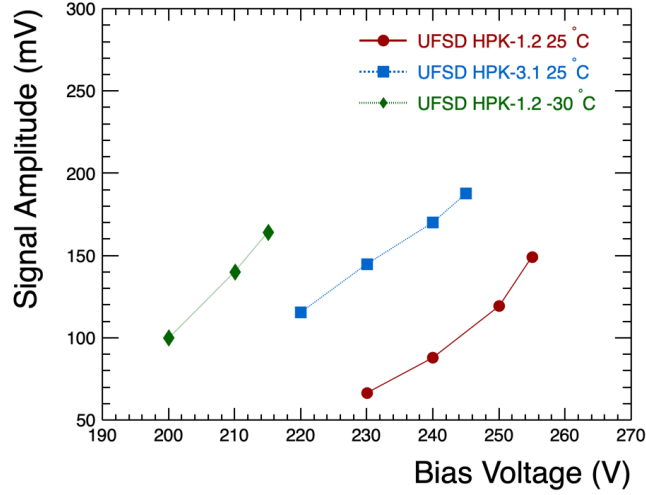


Figure 10: The pulse signal amplitude as a function of bias voltage.

6.3. Noise and Jitter

The noise at different bias voltages is shown in figure 11. The noise usually remains stable in the range of 2.5-4.5 mV throughout the beam test. The signal to noise ratio (SNR) increases with bias voltage and subsequently with the sensor's gain.

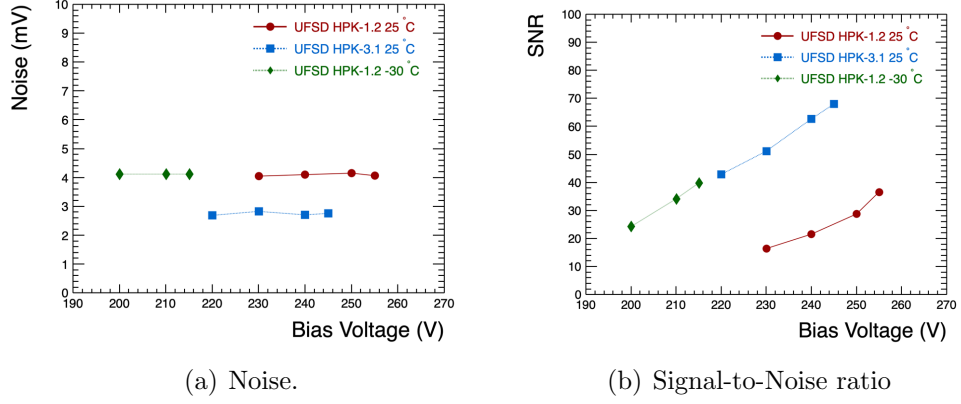


Figure 11: The Noise as a function of bias voltage.

Figure 12 shows the jitter as a function of bias voltage. It shows that the jitter decreases with increasing bias voltage. The contribution is higher at the beginning and end of the pulse because of lesser steepness of pulse.

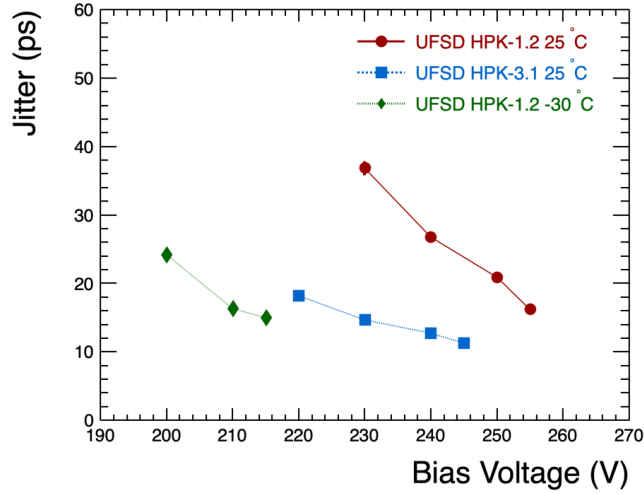


Figure 12: The Jitter as a function of bias voltage.

6.4. Rise Time

The rise-time is a crucial parameter in defining the timing resolution of the UFSD, and it is determined by the drift time of the electrons. The rise-time is the time taken by the signal pulse to reach 90% of maximum signal amplitude from 10%. The decreasing trend of the rise-time indicates an increase in gain with bias voltage due to which the drift velocity inside the bulk increases. A similar effect observed while going from room temperature to low temperature measurements. Figure 13 shows the rise-time at different bias voltages for HPK-1.2 and HPK-3.1. The rise-time decreases with bias voltage for HPK-3.1. Whereas, for HPK-1.2, the rise-time increases slightly, indicating delay due to the multiplication mechanism at higher gain.

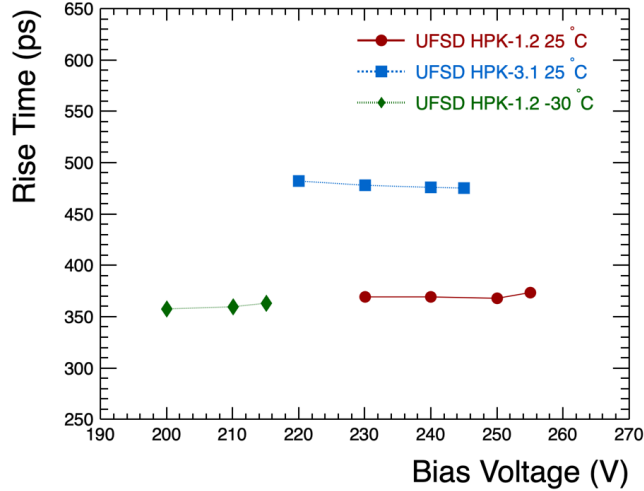


Figure 13: The rise time as a function of the bias voltage.

6.5. Timing Measurements

The timing resolution as a function of the CFD fraction is shown in figure 14. The measured timing resolution is stable above $\sim 15\%$ up-to 80% of CFD fraction. The timing resolution of each of the LGADs described in Section 3.1 has been obtained using the CFD method and shown in figure 15. The results show timing performance at room temperature as well as at -30 °C.

In the beam test, 3 LGADs are used as DUTs, and 4th LGAD is used as a trigger. The time resolution is calculated for ten sets of DUT combinations. The time differences from different combinations of DUTs and TRG are,

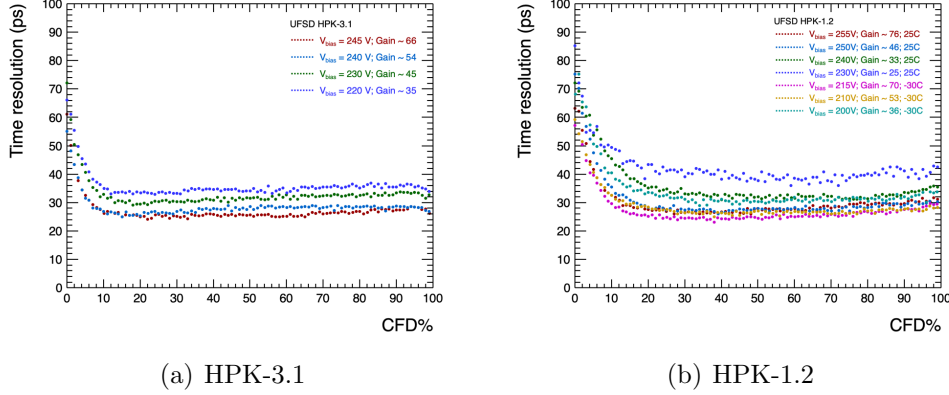


Figure 14: Timing measurement as a function of CFD fraction for HPK-3.1 at room temperature (left) and HPK-1.2 at room temperature and at -30 °C (right).

$\Delta(t_{DUT} - t_{DUT'})$: Three sets of time difference between pairs of DUTs.

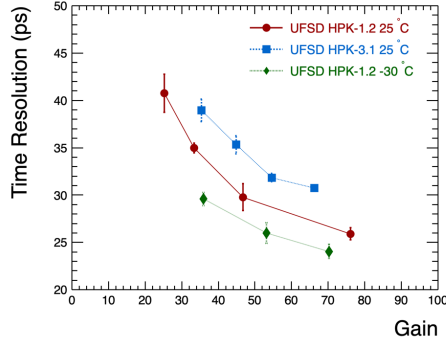
$\Delta(t_{DUT} - t_{TRG})$: Three sets of time difference between DUT and the trigger.

These are the time differences calculated using single DUT, so called as "singles".

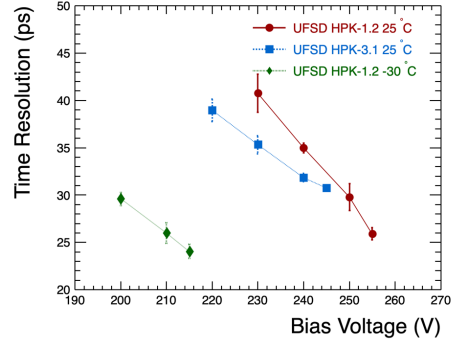
$\Delta(t_{\langle 2DUT \rangle} - t_{TRG})$: Three sets of time difference between average of pair of DUTs and the trigger. As the time difference is taken for average of two UFSds they are called as "Doublets".

$\Delta(t_{\langle 3DUT \rangle} - t_{TRG})$: The time difference between average of three DUTs and the trigger gives the "triplet" measurement.

The results for these measurements are shown in figure 16 and tabulated in table 2 for three different operating conditions. It has been seen that results are very well in agreement with the expectation; $\sigma(N) = 1/\sqrt{N}$. The timing resolution of $14.73 \pm xx$ is measured from a triplet of UFSds operated with a bias voltage of 215V at -30 °C, which is fastest reported time resolution for UFSds till date at the test beam.

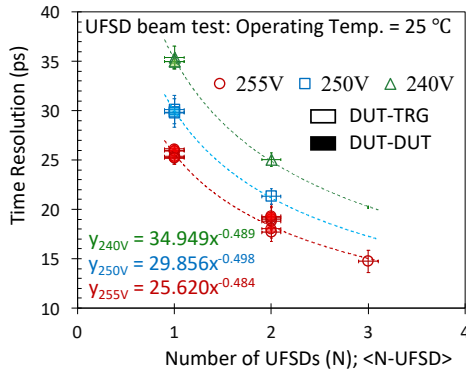


(a) Timing resolution vs. gain

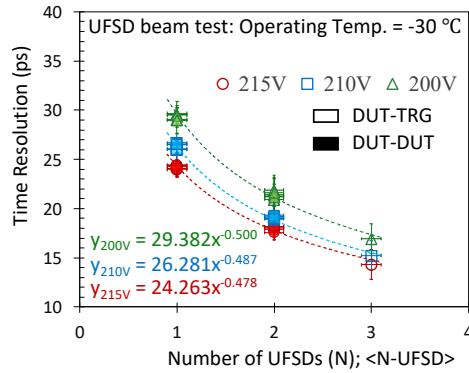


(b) Timing resolution vs. bias voltage

Figure 15: Timing measurement of UFSDs using time-of-flight (TOF) technique for minimum ionising particles (MIP).



(a) 25 °C



(b) -30 °C

Figure 16: The timing resolutions at different bias voltages as a function of the number of UFSDs combined. The data reports measurements for the HPK-1.2 at room temperature and -30 °C (enclosure air temperature) with a 120 GeV proton beam at the Fermilab Test Beam Facility. The missing data point (for $V_{bias} = 240V$ and $N = 3$) is due to the failure of power supply to DAQ during the test beam run.

Table 2: The timing resolution for sets of UFSDs; a single (N=1), a pair (N=2), and the triplet (N=3). The data reports measurements for the HPK-1.2 with a 120 GeV proton beam at the Fermilab Test Beam Facility. The missing data point (for $V_{bias} = 240V$ and $N = 3$) is due to the failure of power supply to DAQ during the test beam run.

Number of DUTs	UFSD Timing Resolution (ps)		
	$V_{bias} = 240\text{ V}$ ($T = 25\text{ }^{\circ}\text{C}$)	$V_{bias} = 255\text{ V}$ ($T = 25\text{ }^{\circ}\text{C}$)	$V_{bias} = 215\text{ V}$ ($T = -30\text{ }^{\circ}\text{C}$)
N = 1	35.12 ± 1.03	25.63 ± 0.52	24.22 ± 0.72
N = 2	25.05 ± 0.69	18.67 ± 1.15	18.01 ± 0.94
N = 3	-	14.73 ± 1.17	14.31 ± 1.52

7. Conclusions

The UFSDs are tested for timing resolutions with the 120 GeV proton test beam at Fermilab Test Beam Facility. The single LGAD sensor with 35 μm thickness and active area of $1.3 \times 1.3\text{ mm}^2$ provided a timing resolution of $35.12 \pm 1.03\text{ ps}$ and $25.63 \pm 0.52\text{ ps}$ at 240 V and 255 V respectively at room temperature. The same LGAD sensor's timing performance was improved to $24.22 \pm 0.72\text{ ps}$ when operated at $-30\text{ }^{\circ}\text{C}$. In the test beam, a telescope comprising four UFSD planes was tested successfully demonstrating improvement on timing resolution given by the relation $1/\sqrt{N}$, where N is the number of UFSDs. When three planes are averaged (triplet), the timing performance of about 14.31 ± 1.52 is measured at a bias voltage of 215 V and at temperature $-30\text{ }^{\circ}\text{C}$, which is the fastest reported timing performance to date. It is observed that the targeted timing response of 10 ps is achievable with an optimized number of layers and thickness of LGAD sensors.

8. Acknowledgements

The work is supported by Laboratory Directed Research and Development (LDRD) funding from Argonne National Laboratory, provided by the Director, Office of Science, of the U.S. Department of Energy under Contract No. DE-AC02-06CH11357. The LDRD project name is "Tomography at an Electron-Ion Collider: Unraveling the Origin of Mass and Spin". Argonne National Laboratory's work is supported by the U.S. Department of Energy,

Office of Science, Office of Nuclear Physics, Office of High Energy Physics, under contract DE-AC02-06CH11357.

This document is prepared using the resources of the Fermi National Accelerator Laboratory (Fermilab), a U.S. Department of Energy, Office of Science, Fermi Lab Test Beam Facility. Fermilab is managed by Fermi Research Alliance, LLC (FRA), acting under Contract No. DE-AC02-07CH11359.

We are thankful to Thomas O'Connor and his team at Physics division, Argonne National Laboratory for their help in fabricating the alignment box. We also like to acknowledge the help provided by Michelle Jonas and Humberto Gonzalez at Silicon Detector Facility, Fermilab in wire-bonding LGAD sensors onto the read-out boards.

References

- [1] H. F.-W. Sadrozinski, A. Seiden, N. Cartiglia, 4d tracking with ultra-fast silicon detectors, Reports on Progress in Physics 81 (2) (2017) 026101. doi:10.1088/1361-6633/aa94d3.
URL <https://iopscience.iop.org/article/10.1088/1361-6633/aa94d3>
- [2] G. Pellegrini, et al., Technology developments and first measurements of low gain avalanche detectors (lgad) for high energy physics applications, Nucl. Instrum. Meth. Sec. A 765 (2014) 12 – 16. doi:<https://doi.org/10.1016/j.nima.2014.06.008>.
URL <http://www.sciencedirect.com/science/article/pii/S0168900214007128>
- [3] N. Cartiglia, et al., Beam test results of a 16 ps timing system based on ultra-fast silicon detectors, Nucl. Instrum. Meth. Sec. A A850 (2017) 83–88. arXiv:1608.08681, doi:10.1016/j.nima.2017.01.021.
URL <http://www.sciencedirect.com/science/article/pii/S0168900217300219>
- [4] H. F.-W. Sadrozinski, et al., Ultra-fast silicon detectors, Nucl. Instrum. Meth. Sec. A 730 (2013) 226 – 231. doi:<https://doi.org/10.1016/j.nima.2013.06.033>.
URL <http://www.sciencedirect.com/science/article/pii/S0168900213008589>

- [5] J. Repond, TOPSiDE: Concept of an EIC Detector, PoS DIS2018 (2018) 179. doi:10.22323/1.316.0179.
- [6] W. Armstrong, Going topside at the eic, 2018 JLab Users Group Meeting <https://www.jlab.org/conferences/ugm/2018/talks/monday/armstrong.pdf> (2018/06/18).
- [7] S. Joosten, Eoi contributed presentation: Argonne national lab, The 2020 Electron-Ion Collider User Group Meeting <https://indico.bnl.gov/event/7352/contributions/39726/> (2020/07/16).
- [8] J. Repond, S. Chekanov, M. Jadhav, J. Metcalfe, T. Shin, TOPSiDE, PoS DIS2019 (2019) 236. doi:10.22323/1.352.0236.
- [9] A. Accardi, et al., Electron Ion Collider: The Next QCD Frontier: Understanding the glue that binds us all, Eur. Phys. J. A 52 (9) (2016) 268. arXiv:1212.1701, doi:10.1140/epja/i2016-16268-9.
- [10] H.-W. Sadrozinski, et al., Sensors for ultra-fast silicon detectors, Nucl. Instrum. Meth. Sec. A 765 (2014) 7 – 11. doi:<https://doi.org/10.1016/j.nima.2014.05.006>.
URL <http://www.sciencedirect.com/science/article/pii/S0168900214005051>
- [11] N. Cartiglia, Signal formation and timing in lgad sensors, AIDA-2020 First annual meeting <https://indico.cern.ch/event/468478/contributions/2135146/> (2016/06/13).
- [12] R. Arcidiacono, Development of ufsd thin silicon sensors for timing applications, Workshop on picosecond timing detectors for physics and medical applications <https://indico.cern.ch/event/565957/contributions/2286360/> (2016/09/16).
- [13] H.-W. Sadrozinski, et al., Ultra-fast silicon detectors (ufsd), Nucl. Instrum. Meth. Sec. A 831 (2016) 18 – 23. doi:<https://doi.org/10.1016/j.nima.2016.03.093>.
URL <http://www.sciencedirect.com/science/article/pii/S0168900216301279>
- [14] Y. Zhao, Others, Comparison of 35 and 50 μ m thin hpk ufsd after neutron irradiation up to $6 \times 10^{15} \text{ n}_{eq} \text{ cm}^2$, Nucl. Instrum. Meth. Sec. A 924 (2019)

- 387 – 393. doi:<https://doi.org/10.1016/j.nima.2018.08.040>.
 URL <http://www.sciencedirect.com/science/article/pii/S0168900218309938>
- [15] S. Mazza, et al., Properties of FBK UFSDs after neutron and proton irradiation up to $6 \cdot 10^{15} \text{ n}_{eq} \text{ cm}^2$, Journal of Instrumentation 15 (04) (2020) T04008–T04008. doi:[10.1088/1748-0221/15/04/t04008](https://doi.org/10.1088/1748-0221/15/04/t04008).
 URL <https://doi.org/10.1088/1748-0221/15/04/t04008>
- [16] N. Minafra, et al., Test of ultra fast silicon detectors for picosecond time measurements with a new multipurpose read-out board, Nucl. Instrum. Meth. Sec. A 867 (2017) 88 – 92. doi:<https://doi.org/10.1016/j.nima.2017.04.032>.
 URL <http://www.sciencedirect.com/science/article/pii/S0168900217304825>
- [17] A. Seiden, et al., Potential for Improved Time Resolution Using Very Thin Ultra-Fast Silicon Detectors (UFSDs) (6 2020). arXiv:2006.04241.
- [18] R. Padilla, et al., Effect of deep gain layer and Carbon infusion on LGAD radiation hardness (4 2020). arXiv:2004.05260.
- [19] G. Kramberger, A. Howard, Z. Kljun, I. Mandic, M. Mikuz, V. Cindro, Annealing effects on operation of thin Low Gain Avalanche Detectors (5 2020). arXiv:2005.14556.
- [20] X. Yang, et al., Layout and Performance of HPK Prototype LGAD Sensors for the High-Granularity Timing Detector (3 2020). arXiv:2003.14071.
- [21] "fermilab test beam facility," [online]., Available: <https://ftbf.fnal.gov> (2020/03).
- [22] N. Cartiglia, et al., Design optimization of ultra-fast silicon detectors, Nucl. Instrum. Meth. Sec. A 796 (2015) 141 – 148. doi:<https://doi.org/10.1016/j.nima.2015.04.025>.
 URL <http://www.sciencedirect.com/science/article/pii/S0168900215004982>

- [23] Z. Galloway, et al., Properties of hpk ufsd after neutron irradiation up to $6 \cdot 10^{15} \text{ n}_{eq} \text{ cm}^2$, Nucl. Instrum. Meth. Sec. A 940 (2019) 19 – 29. doi:<https://doi.org/10.1016/j.nima.2019.05.017>.
URL <http://www.sciencedirect.com/science/article/pii/S0168900219306278>
- [24] A. G. Chynoweth, Ionization rates for electrons and holes in silicon, Phys. Rev. 109 (1958) 1537–1540. doi:[10.1103/PhysRev.109.1537](https://doi.org/10.1103/PhysRev.109.1537).
URL <https://link.aps.org/doi/10.1103/PhysRev.109.1537>